Egypt. J. Chem. **Vol. 66**, No. SI: 13 pp. 187 - 197 (2023)

Egyptian Journal of Chemistry

http://ejchem.journals.ekb.eg/

Kinetic and Thermodynamic Parameters of ^{99}Mo Sorption on Zirconia Nanoparticles Prepared By Hydrothermal Method

E.A. Azooz [1], H.E. Ramadan [1], M. A. Abd Elaal [1], M. A. El-Amir [1], M. A. EL-Absy [1], W. H. Mahmoud [2]

[1] *Radioactive Isotopes and Generators Department, Hot Labs Center, Egyptian Atomic Energy Authority, P.O. Box 13759, Cairo, Egypt*

[2] *Chemistry Department, Faculty of Science, Ain Shams University, Cairo, Egypt*

Abstract

Hydrous zirconium nano-particles (HZN) were prepared by combining two suggested methods, hydrolysis from emulsion solutions followed by hydrothermal treatment to obtain the samples in powder form. Characterization of the prepared nano-particles was performed. According to XRF analysis, ZrO_2 represents 99.5 wt % as the major component of the prepared samples. The particle size of the prepared nano-particle ranged from 40 to 100 nm determined by TEM analysis. DLS analysis shows the average hydrodynamic diameter is 48.3 nm and 72.06 nm for HZN-1 and HZN-2, respectively. The sorption characteristics of ^{99}Mo on hydrous zirconia nano-particles were investigated using a batch experiment technique. The pseudo-second-order kinetic model showed excellent kinetic data fitting (R^2 = 0.99873 and 0.99961 for HZN-1 and HZN-2 nanoparticles, respectively). According to Arrhenius plots, the activation energy of Mo(VI) sorption onto HZN-1 and HZN-2 was found to be 31.8 kJ/mol and 32.5 kJ/mol, respectively. From the Langmuir adsorption isotherm, the maximum sorption capacity is 275.5 and 270.3 mg g^{-1} for HZN-1 and HZN-2, respectively. Thermodynamic functions, the change of free energy (ΔG^0), enthalpy (ΔH^0), and entropy (ΔS^0) of sorption were also calculated. These parameters show that the sorption process is spontaneous and endothermic at 25–50 ◦C.

Keywords: hydrothermal, hydrous Zirconium oxide Nano powder, Thermodynamic functions, Kinetic models, Adsorption isotherms, Activation energy, Molybdenum (VI)–^{99}Mo

1. Introduction

The continuously growing demand for ^{99m}Tc in many countries is a permanent challenge to develop procedures suited for large-scale production of ^{99}Mo, the parent nuclide of ^{99m}Tc, by using conventional research reactors [1]. There are two routes for ^{99}Mo production in nuclear reactors; fission (via the reaction ^{235}U(n,f)^{99}Mo) and activation (via the reaction ^{98}Mo(n,γ)^{99}Mo] [2]. The adsorption of ^{99}Mo radionuclide on a chromatographic column filled with alumina resin is still the most commonly type of ^{99m}Tc-generator used [3]. One of the great disadvantages of the alumina column is its low adsorption capacity for ^{99}Mo [4]. The adsorption capacity of alumina is 20 mg Mo/g alumina at a pH lower than 4.5 and decreases to 2.0 mg Mo/g alumina at pH 4.5-5.0 [5]. Therefore, it is necessary to use high specific activity ^{99}Mo radionuclide, obtained either by irradiation of enriched ^{98}Mo or as a fission product of ^{235}U. Enforce attempts in the development of high capacity sorbents capable of adsorbing much larger quantities of ^{99}Mo carrying out in progress, such as the poly zirconium compound (PZC) [6], poly titanium oxychloride [7], functionalized alumina, nano alumina, nano zirconia, and nano mixed oxides of tetra valent metals (mixed nano crystalline zirconia and titanium) [8]. This strategy is promising to prepare column-based generators using the (n,γ)^{99}Mo. field of nano-sized materials has most the attention of scientists in several fields in recent years. Due to the high surface area and notable surface reactivity, nano materials-based sorbents have higher sorption capacity and selectivity compared to conventional adsorbents such as alumina and similar oxide species. The high surface area is advantageous for realizing high capacity facilitating enhanced

*Corresponding author e-mail: hala_ramadan2013@yahoo.com. (H.E. Ramadan)
EJCHEM use only: Received date 25 June 2022; revised date 17 September 2022; accepted date 01 October 2022
DOI: 10.21608/EJCHEM.2022.146915.6376

loading of ^{99}Mo and allowing the use of low specific activity ^{99}Mo. Several nanomaterial-based sorbents have been reported for the preparation of chromatographic radionuclide generators using (n,γ)^{99}Mo [9]–[11].

Zirconium dioxide, commonly known as zirconia, is an interesting inorganic material and is receiving more attention in recent years due to its excellent mechanical and chemical [12], stability, and extraordinary range of chemical and physical properties, including the properties of bulk and surface layer [13]. Several techniques are available for the preparation of zirconium dioxide nanoparticles, such as sol/gel [14], vapor phase [15], pyrolysis [16], spray pyrolysis [17], hydrolysis [18], hydrothermal l[19], and microwave plasma [20]. However, many limitation factors, such as complications, high reaction temperature, long reaction time, toxic reagents, and high cost of production, are faced with these methods making a difficulty to the preparation of zirconia nanoparticles on a large-scale [21]. Researchers, materials scientists, and engineers have made significant developments to ease and improve the methods of preparation of zirconia nanoparticles [22].

This work aims to the preparation of hydrous zirconia nano particles gel by combining two suggested methods, hydrolysis from emulsion solutions followed by hydrothermal treatment. Then, study the ^{99}Mo sorption behavior from aqueous solution on the obtained zirconia nano particle by static methods to elucidate the kinetics and thermodynamics parameters of ^{99}Mo sorption.

2. EXPERIMENTAL

2.1. Chemical reagents and instruments

All the chemicals used in this work were of AR grade. Distilled water was used for the preparation of all solutions and washing purposes. Molybdenum trioxide (Sigma- Aldrish), zirconyl chloride (Sigma- Aldrish), isoamyl alcohol, 95% (oxford) ammonia solution, 28-30% (BDH), and hydrochloric acid, 37% (BDH) were used without further purification.

Gas-tight hydrothermal reactors made of S316 stainless steel with 200-mL PTFE (Teflon) inner chambers (autoclaves), were used for hydrothermal preparation processes.

A γ-ray spectrometer composed of a multichannel analyzer (MCA) of the Inspector 2000 model (Canberra Series, USA), coupled with high-purity germanium (HPGe) coaxial detector of the GX2518 model, was used for the γ-radioactivity identification and measurement.

The FT-IR spectra were recorded by using an FT-IR spectrometer (MB157S model, Bomem, Canada) from 4000 to 400 cm^{-1}.

Thermal analysis for the prepared sample, including simultaneous TGA and DTA, was carried out using a thermal analyzer instrument (DTG-60H model, Shimadzu, Japan).

Zetasizer (Zetasizer Nano ZS/ ZEN3600, Malvern Instruments Ltd., UK) was used to determine hydrodynamic diameter distribution, via dynamic light scattering (DLS), and Zeta potential, via electrophoretic light scattering (ELS), of the nanoparticles of the synthesized gel materials.

The morphology of the prepared material was characterized using a field emission scanning electron microscope (FESEM) (JSM-6510A, Japan).

X-ray diffraction patterns (XRD) were performed with an 18 kV diffractometer (Bruker, D8 Advance model, USA) with monochromatic Cu Kα radiation (λ=1.542 Å).

Elemental analysis was carried out using an X-ray fluorescence spectrometer (Philips XRF, BW-1200 sequential spectrometer, Netherlands).

2.2. Radioactive ^{99}Mo tracer solutions

The stock solution of molybdenum labeled with ^{99}Mo was prepared by dissolving the inactive MoO_3 in NaOH solution containing 1.0 ml of carrier-free ^{99}Mo radiotracer (Fission ^{99}Mo as $Na_2{}^{99}MoO_4$ in 0.1 M NaOH solution obtained from Radioisotope Production Facility, ETRR-II, Egyptian Atomic Energy Authority).

2.3. Preparation of hydrous zirconium oxide nanoparticles (HZN-1 and HZN-2).

8.125 g of zirconium oxychloride was dissolved in 100 mL 80% isoamyl alcohol (for HZN-1)) and 100 ml 80% propanol alcohol (for HZN-2) as a capping agent, to prevent aggregates and finally obtained a nano-sized particle [22], [23]. 20% ammonia solution was added as a pore-forming agent, to obtain a porous material with a large surface area [24], drop by drop with vigorous stirring by a magnetic stirrer till the pH of the final mixture solution reached 7.0-8.0. The solution and precipitate mixture was placed in Teflon chambers of hydrothermal reactors (autoclaves). Then, the mixture fractions were autoclaved at 160 ± 1.0 °C for 4 h in the case of HZN-1 and 100 ± 1.0 °C for 24 h in the case of HZN-2. After digestion in an autoclave, separation was carried out by centrifugation at speed of $3.0x10^3$ rpm for 10 ± 0.1 min. The obtained precipitate was thoroughly washed with distilled water and re-centrifuged for phase separation. Then, the precipitate was dried at 50 ± 1.0 °C for 24 h,

washed three times with distilled water, and then re-dried at 50 ± 1.0 °C until constant weight.

2.4. Batch experiments

Batch experiments were carried out by mixing in closed vials 10.0 mL fractions of ^{99}Mo solutions of different concentrations ($1x10^{-3}$, 5×10^{-3}, $1x10^{-2}$, 5×10^{-2}M) and 0.1g of the prepared samples (hydrous zirconium oxide nanoparticles, HZN-1 or HZN-2) at pH~ 2.0, HCl acid solution, in a thermostatic water bath at different temperatures (25, 40, and 50 ± 1.0 ^{o}C). Percent uptake of ^{99}Mo was followed at different time intervals using the following Equation:

$$U\% = \frac{C_0 - C_e}{C_0} \times 100 \quad (1)$$

were, U is percent uptake of ^{99}Mo, C_0 and C_e are the count rates (cpm) of 740-keV peak of ^{99}Mo in 1.0 ml of the aqueous solution before contact with hydrous zirconium oxide nanoparticles sample and after attainment of equilibrium, respectively [25].

2.5. Kinetic studies

Isothermal batch adsorption studies$5x10^{-3}$ M molybdate-^{99}Mo (Cl^- medium at pH2) batch adsorption ontoHZN-1 and HZN-2 at 25, 40, and 50^{o}C to determine the best kinetic model(s) representing the adsorption process and to determine activation energy.

2.6. Adsorption isothermal studies

Isothermal batch adsorption studies of $1x10^{-4}$- $5x10^{-2}$ M molybdate (VI) (Cl^{-2} medium at pH2) onto HZN-1 and HZN-2 at 25^{o}C were concluded to determine the best adsorption isothermal process and determine the thermodynamic ($\Delta H^{\bullet}$, $\Delta S^{\bullet}$, $\Delta G^{\bullet}$).

3. RESULTS AND DISCUSSION

3.1. Characterization of hydrous zirconium oxide nanoparticles

The prepared hydrous zirconium oxide nanoparticles (HZN-1 and HZN-2) are in the form of white fine particle in which ZrO_2 represent 99.5 wt % as the major component of the prepared samples, determined by X-ray fluorescence (XRF) analysis.

According to dynamic light scattering data (Figures 1, a, and b), it was found that the average hydrodynamic diameter is 48.3 nm (95.3 % of the particle) and 72.06 nm (96.3 % of the particle) for HZN-1 and HZN-2, respectively.

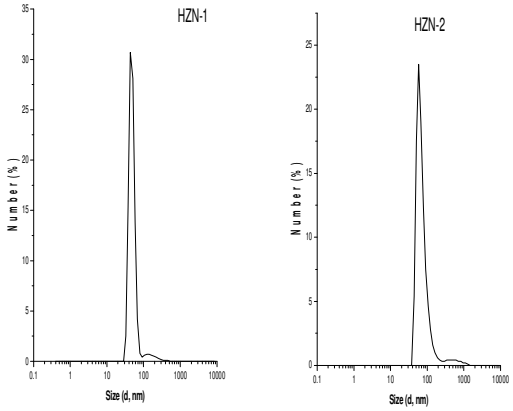

Figure (1): Hydrodynamic size distribution of the prepared hydrous zirconium oxide nanoparticles

Figure (2) shows FT-IR spectra of the prepared HZN-1 and HZN-2 nanoparticles dried at 50 ± 1.0 °C. The absorption bands around 3400 cm^{-1} and 1630 cm^{-1} correspond to stretching and bending frequencies of the O-H group present in the prepared samples, which means the presence of water molecules in the two samples. The spectra show an absorption band around 1350 (1342 for HZN-1 and 1378 for HZN-2) which may be related to adsorbed CO_2 from the atmosphere [26]. The absorption bands in the range of 500-700 cm^{-1} may be attributed to the Zr-O vibration mode [27].

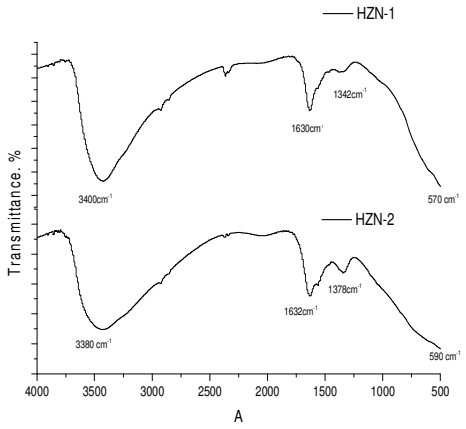

Figure 2: FT-IR spectra of the prepared hydrous zirconium oxide nanoparticles

Figure (3) shows thermo-gravimetric analysis (TGA) and differential thermal analysis (DTA) curves for HZN-1 and HZN-2 nanoparticles. The thermo-gravimetric curves show continuous

irreversible total weight loss in the order of 21.7 and 17.8% with increasing the heating temperature from 50 up to 1000 °C, for HZN-1 and HZN-2, respectively. Also, the total weight loss decreased in the case of propanol media (i.e. HZN-2) than iso-amyl media (HZN-1) which is compatible with IR data mentioned before. Differential thermal analysis curves show that the two samples exhibited initial weight loss in the temperature range from ~ 80 to 200 °C due to loss of free water [28] in the form of two broad endothermic peaks corresponding to 16.5 and 12% for HZN-1and HZN-2, respectively. The weights losses from 200 to 450 were assigned to losses of water of hydration and water of crystallization [28]. The DTA curves show exothermic peaks around 450 °C (450 for HZN-1and 440 for HZN-2). This peak may be assigned to the transformation of hydrous zirconium oxide powder from an amorphous shape to a crystalline shape [28].

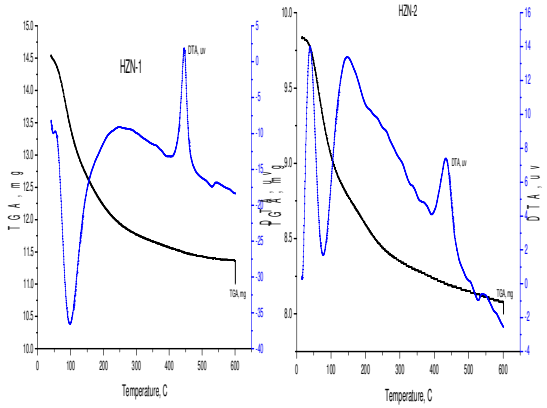

Figure 3: TGA and DTA curves of the prepared hydrous zirconium oxide nanoparticles

As shown in FESEM surface images (Figure 4), the prepared hydrous zirconium oxide nanoparticle appeared mainly in the form of a mixture of distorted circular plates randomly distributed among big-sized rocky piles. The plates appear in the form of undistorted variable particles size. The two images show meanders and cavities.

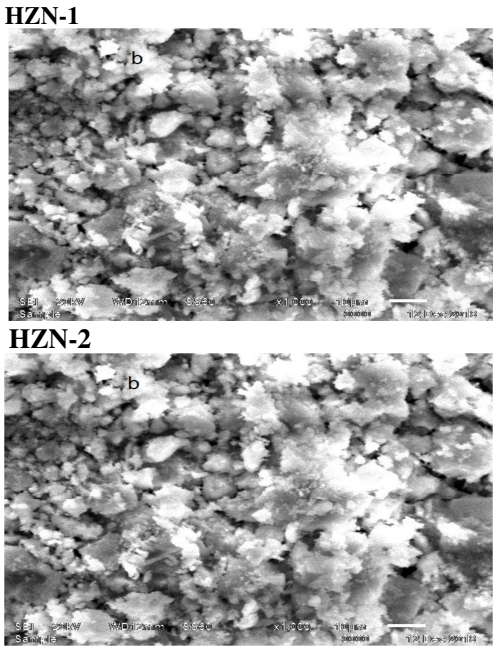

Figure 4: FESEM surface images of the prepared hydrous zirconium oxide nanoparticles

According to Figure 5, X-ray diffraction patterns of the HZN-1 and HZN-2 nanoparticles indicate the completely amorphous nature of the obtained particles independently of the method of preparation used.

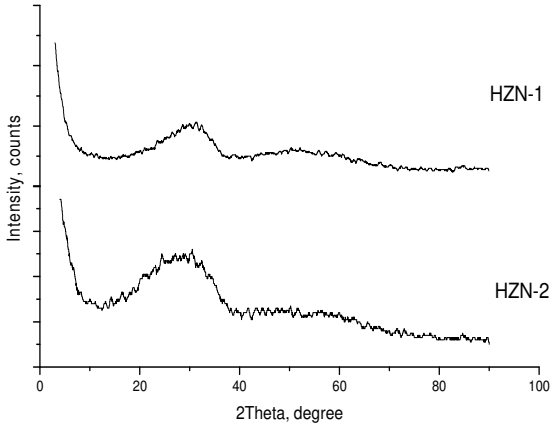

Figure 5: X-ray diffraction patterns of the prepared hydrous zirconium oxide nanoparticles

According to Figures (6 a and b), the zeta potential (mV) of the prepared hydrous zirconia nanoparticles in water as a dispersed phase was found to be +26.6 mV and +32.9 mV for HZN-1 and HZN-2, respectively.

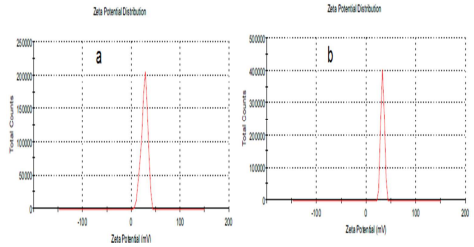

Figure 6: Zeta potential (mV) of the prepared hydrous zirconium oxide nanoparticles (a) HZN-1 and (b) HZN-2

TEM micrographs of the prepared HZN-1 and HZN-2 nanoparticles are shown in Figure (7). Microscopic examinations of the prepared HZN-1 and HZN-2 zirconia nanoparticles show semispherical nanoparticles and most of these particles have a slightly irregular form with particles size ranging from 40 to 100 nm. The range is consistent with the particle sizes determined by the DLS, as shown in Figure (1).

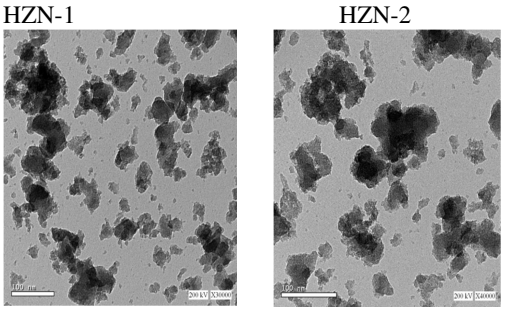

Figure 7: TEM images of the prepared hydrous zirconium oxide nanoparticles

3.2. Sorption studies of ^{99}Mo onto the prepared hydrous zirconium oxides

3.2.1. Effect of pH values

The M-OH functional groups contained in these structure of hydrous zirconium oxide nano- particles show amphoteric reactions depending on the pH value of the solution and give rise to anion exchange in the acid medium or cation exchange in the basic medium[29]. A comparison of the sorption behavior of HZN-1 and HZN-2 seemed a practical way to find a suitable HZN for sorption of various molybdate ions built in the acidified solutions depending on pH value and Mo concentration[30], [31]

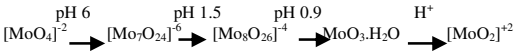

The influence of pH on the sorption of $5x10^{-3}$ M ^{99}Mo ions onto HZN-1 and HZN-2 nanoparticles is shown in Figure (8). HZN-1and HZN-2 nanoparticles exhibited a high sorption affinity for ^{99}Mo ions, especially in an acidic medium. For HZN-1and HZN-2 nanoparticles, the uptake percent of ^{99}Mo ions attained the maximum value at pH of 1.0 – 4.0. Then the uptake percent of ^{99}Mo ions decreases by increasing the pH value till reaches the minimum value at pH 9.0 as shown in figure 8. After contacting the molybdate solutions with the HZN-1 and HZN-2, the pH changed to a higher pH value than the original one in the case of pH value from 1-4, while the pH value was changed to a lower value in the case of pH $\geq$ 4.0. This may be due to the liberation of the OH^- group in acid media to change with molybdate ions. The Mo-sorption on HZN may be explained by anion exchange and electrostatic mechanism.

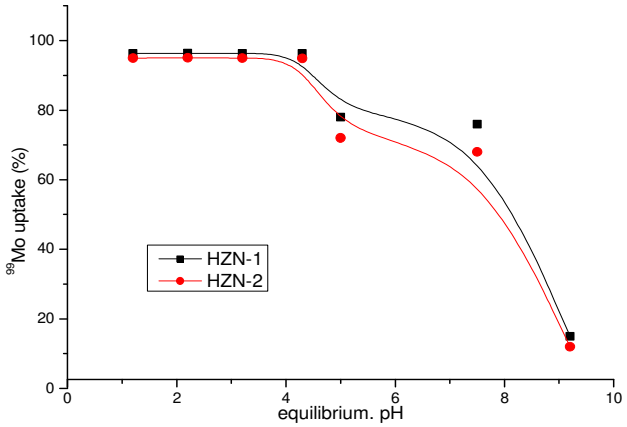

Figure 8: Influence of equilibrium pH on the sorption of $5x10^{-3}$ M ^{99}Mo onto hydrous zirconium oxide, HZN-1 and HZN-2, nano particles at ambient room temperature, ~ 25C

3.2.2. Effect of contact time

The influence of contact time in $5x10^{-3}$ M ^{99}Mo sorption onto HZN-1 and HZN-2 nanoparticles is shown in Figure (9). It can be seen that, the sorption efficiency of ^{99}Mo increases with increasing shaking time. The percent uptake of ^{99}Mo reaches the maximum value of 96.5 % and 95.3 % after a contact time of 24 h for HZN-1 and HZN-2, respectively.

3.4 Effect of temperature

The effect of temperature on the sorption of $5x10^{-3}$ M molybdenum on HZN-1 and HZN-2 zirconium oxide nanoparticles was also investigated using the optimized conditions. The sorption of ^{99}Mo at 293, 313, and 323 was found to be 96.45, 97.4, and 98.48% for HZN-1 and 95.3, 97.49, and 98.31% for HZN-2, respectively. The increase in the amount of

sorbed molybdenum with the increasing temperature may be due to the increase in the mobility of the ionic species present in the solution at higher temperatures.

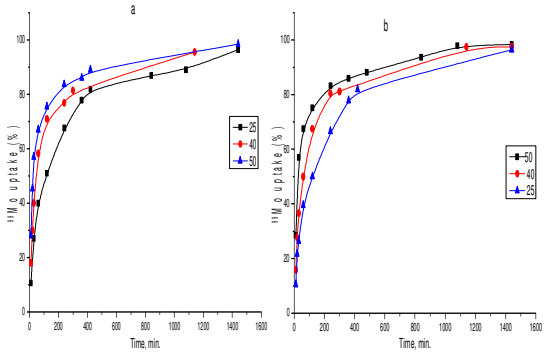

Figure 9: uptake of ^{99}Mo onto hydrous zirconium oxide, (a) HZN-1 and (b) HZN-2, with an initial ^{99}Mo concentration of 5x10^{-3} M at different temperatures

3.5 Sorption kinetics

To investigate the controlling mechanism of the adsorption process such as mass transfer and chemical reaction, the pseudo-first-order and pseudo-second-order equations are applied to model the kinetics of molybdenum sorption on hydrous zirconium nano particles.

Lagergren's equation for first-order kinetics can be written as follows [32] :

$$\log(q_e - q_t) = \log q_e - \frac{K_1 t}{2.303} \quad (4)$$

Where q_e and q_t; are the amount of adsorbate adsorbed (mg g^{-1}) at equilibrium and at time t, respectively. K_1 is the rate constant (min^{-1}). Pseudo-first-order kinetic for two prepared gels (HZN-1 and HZN-2) plotted at 25 ◦C is given in Figure (10).

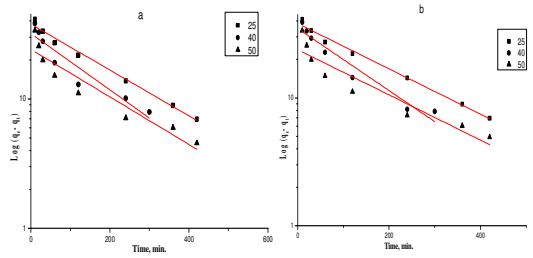

Figure (10): Pseudo-first-order model for sorption of 5x10^{-3} Mo onto hydrous zirconium oxide (a: HZN-1 and b: HZN-2) at different temperatures ^{0}C

The rate constant k_1 and correlation coefficient for molybdenum adsorption at different temperatures were calculated from linear plots of log(q_e-q_t) versus t Figures (10 (a) and (b)) and are listed in Table (1). The correlation for the pseudo-first-order kinetic model is low. Moreover, a large difference in equilibrium adsorption capacity (q_e) between the experimental and calculation was observed, indicating a poor pseudo-first order fit to the experimental data.

Pseudo-second-order reactions are described by the following equation [25], [33] :

$$\frac{t}{q_t} = \frac{1}{k_2\, q_e^2} + \frac{1}{q_e} t \quad (5)$$

Where q_e andq_t: are the sorption capacities of molybdenum (VI) at equilibrium and at time t (mg g^{-1}), respectively. $k_2 q_e^2$: is the initial sorption rate of molybdenum (VI) in the pseudo-second-order model (mg g^{-1} h^{-1}). For the plot t/q_t against t, the slope of the obtained line (equals ($1/q_e$), while the intercept equals ($1/K_2 q_e^2$). Pseudo-second-order kinetic for two prepared gels (HZN-1 and HZN-2) plotted at 25 ◦C is given in Figures (11 (a) and (b)).

The correlation coefficients and q_e values calculated from pseudo 2nd order kinetic model plots at 25, 40, and 50 ºC, were close to the experimental value, as shown in table Table (1).

At all temperatures studied, straight lines with high extremely high correlation coefficient (≥ 0.998) were obtained. In addition, the calculated q_e values are also in agreement with the experimental data. in the case of pseudo-second-order kinetics. These suggest that the adsorption data are well represented by pseudo-second-order kinetics [25].

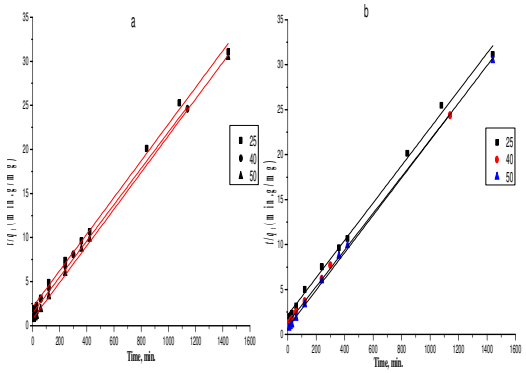

Figure (11): Pseudo-second-order model for sorption of 5x10^{-3} Mo onto hydrous zirconium oxide (a: HZN-1and b: HZN-2) at different temperatures ^{0}C

Table (1)
Calculated parameters of pseudo-first-order and second-order kinetic models and activation energy data for Mo (VI) ion sorbed onto hydrous zirconium oxide nano-particle

Sample	Tem., Kelvin	First-order kinetic parameter			Second-order kinetic parameter			qe, experimental, mg/g
		K_1	qe,cal., mg/g	R^2	K_2	q e,cal, mg/g	R^2	
HZN-1	298	0.0047	51.4	0.73	0.00021	48.1	0.997	46.29
	313	0.0050	31.9	0.88	0.00030	48.7	0.996	46.35
	323	0.0042	24.1	0.88	0.00049	48.4	0.998	47.27
HZN-2	298	0.0046	50.7	0.73	0.000202	48.05	0.996	43.92
	313	0.0056	34.9	0.94	0.000336	49.06	0.999	46.35
	323	0.0040	23.8	0.87	0.000569	48.05	0.998	47.2

Arrhenius plots	Slope		Intercept		Ea, kJ/mol		Adsorption limits, kJ/mol		
	HZN-1	HZN-2	HZN-1	HZN-2	Determined		< 24	24:40	> 40
					HZN-1	HZN-2	physical	Ion exchange	chemical
	-1654.6	-1697.4	1.83	1.97	31.6	32.5			

At all temperatures studied, straight lines with high extremely high correlation coefficient (≥ 0.998) were obtained. In addition, the calculated q_e values are also in agreement with the experimental data. in the case of pseudo-second-order kinetics. These suggest that the adsorption data are well represented by pseudo-second-order kinetics [25].

Figure (12) shows Arrhenius plots of the pseudo-second-order sorption of $5x10^{-3}$ M Mo (VI), which are plots of the sorption rate constant, k_2, against the reciprocal of sorption temperature, 1/T (K^{-1}). The sorption rate constant can be related to the activation energy, Ea (kJ/mol), as indicated by the Arrhenius equation[33]. The linear form of the Arrhenius equation can be represented as:

$$\log k_2 = \log k_0 - \frac{Ea}{2.303RT} \qquad (6)$$

According to Arrhenius plots activation energy of Mo(VI) sorption onto HZN-1 and HZN-2 was found to be 31.8 kJ/mol and 32.5 kJ/mol, respectively (Table 1), indicating the ion exchange mechanism of the adsorption process [34].

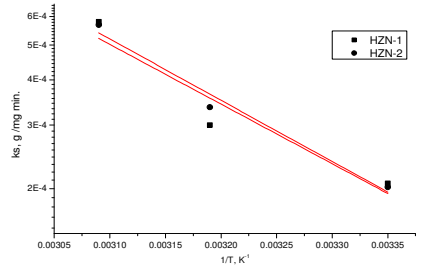

Figure (12): Arrhenius plots of the pseudo-second-order model of adsorption of $5x10^{-3}$ M Mo on HZN-1 and HZN-2.

3.6 Sorption isotherm models.

For thermodynamic considerations in terms of sorption, two commonly used models, namely Langmuir and Freundlich isotherms were tested using the initial concentration dependence data.

The Langmuir equation was tested in the following form[35]:

$$\frac{C_e}{q_e} = \frac{1}{K_L Q_{max}} + \frac{C_e}{Q_{max}} \qquad (7)$$

Where, C_e is the equilibrium concentration of molybdenum (VI)in solution (mg l^{-1}) and q_e is the amount of molybdenum sorbed at equilibrium (mg g^{-1}), Q_{max} is the maximum adsorbed amount of individual molybdenum (VI) ions onto the adsorbent surfaces (mg g^{-1}) and K_L is the Langmuir constant related to the sorption energy coefficient (L mg^{-1}),

As shown in Figure (13), the linear plot of Langmuir adsorption isotherm of ^{99}Mo onto hydrous zirconium oxide nanoparticles(HZN-1 and HZN-2), the correlation coefficient value of the linear plot is satisfactory (R^2 = 0.99601 and 0.99864 for HZN-1 and HZN-2, respectively). The maximum sorption capacity was 275.5 and 270.3 mg g^{-1} for HZN-1 and HZN-2, respectively, and the sorption energy coefficient (4.0 $x10^{-3}$ and $2.0x10^{-3}$ L mg^{-1} for HZN-1 and HZN-2 nanoparticles, respectively) were calculated from the slope and the intercept of the linear plot, respectively.

The sorption data were also tested using Freundlich isotherm equation following:[36].

$$\log q_e = {}^{1}/_{n} \log C_e + \log K_f \quad (8)$$

Where q_e is the amount of molybdenum sorbed at equilibrium (mg g^{-1}), C_e is the equilibrium concentration of molybdenum in solution (mg L^{-1}), K_f is the Freundlich constant (mg/g), the measure of the sorption capacity of the adsorbent, and 1/n is the heterogeneity factor, a constant relating to sorption intensity or surface heterogeneity. Figure (14) shows the linear plot of Freundlich isotherm of Mo-99 sorption on HZN-1 and HZN-2 hydrous zirconium oxide nanoparticles [37], [38]. As shown in table (2), Compared with the correlation coefficient value of the linear plot of Langmuir and Freundlich isotherms, the Freundlich model was found less satisfactory (R^2 = 0.911 and 0.77 for HZN-1 and HZN-2, respectively).

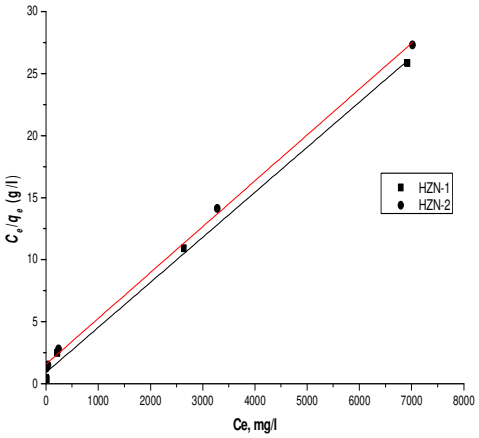

Figure (13): linear plot of Langmuir isotherm of 5x10^{-3} M ^{99}Mo onto hydrous zirconium oxide, HZN-1, and HZN-2

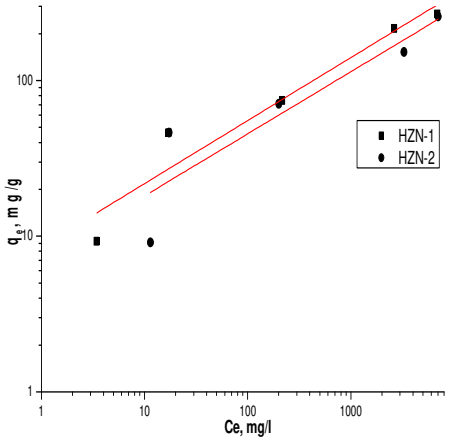

Figure (14): Frindlish isotherm of 5x10^{-3} M ^{99}Mo onto hydrous zirconium oxide, HZN-1, and HZN-2, at 25 ºC

3.7 Sorption thermodynamics

Thermodynamic parameters such as changes in the standard free energy (ΔG^0), enthalpy (ΔH^0), and entropy (ΔS^0) can be calculated using the following equations [39]:

$$K_c = \frac{C_{Ae}}{C_{Se}} \quad (8)$$

$$\ln K_c = \frac{\Delta S^0}{R} - \frac{\Delta H^0}{RT} \quad (9)$$

$$\Delta G^0 = \Delta H^0 - T\Delta S^0 \quad (10)$$

Where K_C is the equilibrium constant, C_{Ae} is the amount of adsorbate on the adsorbent at equilibrium (mg/g), and C_{Se} is the equilibrium concentration of adsorbate in the solution (mg/L).

The amount of Mo-99 adsorbed at equilibrium at different temperatures for 25, 40, and 50 ◦C was used to calculate and obtain thermodynamic parameters. Based on Eqs. (8)–(10), ΔH^0 and ΔS^0 were calculated from the slope and intercept of the linear plot of ln K_C versus 1/T as shown in Figure (15). The values of K_C, ΔG^0, $\Delta H^{0,}$ and ΔS^0 parameters were summarized in Table (3). The change in the standard free energy ΔG^0 with negative values at all the experimental temperatures indicates that ^{99}Mo sorption on hydrous zirconium oxide nanoparticles, HZN-1 and HZN-2, is spontaneous over the temperature range. Furthermore, ^{99}Mo sorption has physical characteristics since the free energy change is between 0 kJ/mol and −20 kJ/mol [40]. The positive value for enthalpy (ΔH^0) indicates the endothermic nature of sorption. The positive value of enthalpy (ΔS^0) indicates that the degree of freedom of ions is increased by sorption and also is an indication of the stability of surface sorption.

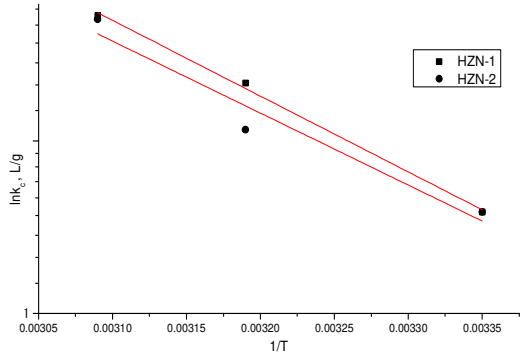

Figure 15: Variation of equilibrium constant (K_C) as a function of temperature

Table (2)
Isotherm models constants and correlation coefficient for adsorption of molybdenum onto hydrous zirconium oxide nano-particle at 25 °C

Sample	Longmuir kinetic parameter			Frindlish kinetic parameter		
	K_L(L.mg^{-1})	Q_{max}, cal.(mg/g)	R^2	K_f (mg/g)	n	R^2
HZN-1	0.004	275 .4	0.99	8.5	2.47	0.91
HZN-2	0.002	270.3	0.99	7.2	2.51	0.77

Table (3)
Calculated parameters of thermodynamic properties of the Mo(IV) ion sorption onto hydrous zirconium oxide nano-particle

Temperature, K	HZN-1				HZN-2			
	R^2	ΔH^0 KJmol^{-1}	ΔS^0 KJmol^{-1}	ΔG^0 KJmol^{-1}	R^2	ΔH^0 KJmol^{-1}	ΔS^0 KJmol^{-1}	ΔG^0 KJmol^{-1}
298				-2.24				-1.06
313	0.995	36.5	0.13	-4.19	0.91	34.7	0.12	-2.86
323				-5.49				-4.06

4. CONCLUSION

Zirconia nanoparticles (HZN-1 and HZN-2) were prepared by combining two suggested methods, hydrolysis from emulsion solutions in alkaline 20 % ammonia solution followed by hydrothermal treatment in a hydrothermal reactor. The prepared materials were characterized through different characteristic techniques and the results showed that the prepared zirconia nanoparticles (HZN-1 and HZN-2) are in the form of white fine particle in which ZrO_2 represent 99.5 wt% as the major component, the average hydrodynamic diameter is 48.3 nm for the HZN-1 and 72.06 nm for the HZN-2 and both HZN-1 and HZN-2 is amorphous in structure. The ^{99}Mo sorption was favored at higher temperatures and slightly initial acid pH values in the equilibrium. The kinetics of ^{99}Mo sorption from aqueous solution on the prepared HZN-1 and HZN-2 follows the pseudo-second-order rate law and obeys the Langmuir isotherms. According to the thermodynamic data and the negative or positive values and magnitudes of ΔH^0, ΔS^0 and ΔG^0 we conclude that the sorption process was endothermic and stable, spontaneous, and ^{99}Mo sorption has physical characteristics. The prepared HZN-1 and HZN-2 can be effectively used as the base material for the sorption of ^{99}Mo for the preparation of ^{99}Mo/^{99m}Tc generators. Further studies will concern the preparation of ^{99}Mo/^{99m}Tc generators based on HZN-1 and HZN-2 as adsorbent materials.

Credit authorship contribution statement
H.E.Ramadan: Conceptualization.
Declaration of competing interest
The authors declare that they have no known competing financial interests or personal relationships that could have appeared to influence the work reported in this paper.

5. REFERENCE

[1] Y. Fujita *et al.*, "Mechanisms Responsible for Adsorption of Molybdate ions on Alumina for the Production of Medical Radioisotopes," *Bull. Chem. Soc. Jpn.*, vol. 95, no. 1, pp. 129–137, 2022.
[2] C. Ma, A. Vasileiadis, H. T. Wolterbeek, A. G. Denkova, and P. S. Crespo, "Adsorption of molybdenum on Zr-based MOFs for potential application in the 99Mo/99mTc generator," *Appl. Surf. Sci.*, vol. 572, p. 151340, 2022.
[3] T. Monir, A. S. El-Din, Y. El-Nadi, and A. Ali, "A novel ionic liquid-impregnated chitosan application for separation and purification of fission 99Mo from alkaline solution," *Radiochim. Acta*, vol. 108, no. 8, pp. 649–659, 2020.
[4] Y. Fujita *et al.*, "Effect on 99Mo-adsorption/99mTc-elution properties of alumina

with different surface structures," *J. Radioanal. Nucl. Chem.*, vol. 327, no. 3, pp. 1355–1363, 2021.
[5] R. Chakravarty *et al.*, "Solid state synthesis of mesoporous alumina: A viable strategy for preparation of an advanced nanosorbent for 99Mo/99mTc generator technology," *Microporous Mesoporous Mater.*, vol. 287, pp. 271–279, 2019.
[6] P. Khongpetch, S. Chingjit, M. Dangprasert, W. Rangsawai, and N. Virawat, "Performance of poly zirconium compound based 99 Mo/99m Tc generator," 2007.
[7] L. Van So, C. D. Nguyen, P. Pellegrini, and V. C. Bui, "Polymeric titanium oxychloride sorbent for 188W/188Re nuclide pair separation," *Sep. Sci. Technol.*, vol. 44, no. 5, pp. 1074–1098, 2009.
[8] J. S. Lee, U. J. Park, K. J. Son, H. S. Han, and S. K. Ryu, "Surface-modified alumina as a high capacity material of 99Mo/99mTc generator column," *Proc. 2007 AIChE Annu. Meet., Salt Lake City, Utah*, 2007.
[9] R. Chakravarty, R. Shukla, R. Ram, A. K. Tyagi, A. Dash, and M. Venkatesh, "Practicality of tetragonal nano-zirconia as a prospective sorbent in the preparation of 99Mo/99mTc generator for biomedical applications," *Chromatographia*, vol. 72, no. 9, pp. 875–884, 2010.
[10] R. Chakravarty, R. Shukla, R. Ram, M. Venkatesh, A. K. Tyagi, and A. Dash, "Exploitation of nano alumina for the chromatographic separation of clinical grade 188Re from 188W: a renaissance of the 188W/188Re generator technology," *Anal. Chem.*, vol. 83, no. 16, pp. 6342–6348, 2011.
[11] R. Chakravarty, R. Ram, A. Dash, and M. R. A. Pillai, "Preparation of clinical-scale 99Mo/99mTc column generator using neutron activated low specific activity 99Mo and nanocrystalline γ-Al2O3 as column matrix," *Nucl. Med. Biol.*, vol. 39, no. 7, pp. 916–922, 2012.
[12] S. Nong *et al.*, "Highly Hydroxylated Porous Nanozirconia for Complete Trace Cr(VI) Removal," *ACS Appl. Nano Mater.*, vol. 3, no. 4, 2020, doi: 10.1021/acsanm.0c00017.
[13] A. Arena *et al.*, "Nanostructured zirconia-based ceramics and composites in dentistry: A state-of-the-art review," *Nanomaterials*, vol. 9, no. 10, 2019, doi: 10.3390/nano9101393.
[14] A. U. Limaye and J. J. Helble, "Effect of precursor and solvent on morphology of zirconia nanoparticles produced by combustion aerosol synthesis," *J. Am. Ceram. Soc.*, vol. 86, no. 2, 2003, doi: 10.1111/j.1151-2916.2003.tb00011.x.
[15] F. Heshmatpour and R. B. Aghakhanpour, "Synthesis and characterization of nanocrystalline zirconia powder by simple sol-gel method with glucose and fructose as organic additives," *Powder Technol.*, vol. 205, no. 1–3, 2011, doi: 10.1016/j.powtec.2010.09.011.
[16] H. Keskinen, P. Moravec, J. Smolík, V. V. Levdansky, J. M. Mäkelä, and J. Keskinen, " Preparation of ZrO 2 fine particles by CVD process: Thermal decomposition of zirconium tert-butoxide vapor," *J. Mater. Sci.*, vol. 39, no. 15, pp. 4923–4929, 2004, doi: 10.1023/b:jmsc.0000035338.85508.cb.
[17] W. Nimmo, D. Hind, N. J. Ali, E. Hampartsoumian, and S. J. Milne, "The production of ultrafine zirconium oxide powders by spray pyrolysis," *J. Mater. Sci.*, vol. 37, no. 16, pp. 3381–3387, 2002, doi: 10.1023/A:1016549325319.
[18] C. Y. Tai, B. Y. Hsiao, and H. Y. Chiu, "Preparation of spherical hydrous-zirconia nanoparticles by low temperature hydrolysis in a reverse microemulsion," *Colloids Surfaces A Physicochem. Eng. Asp.*, vol. 237, no. 1–3, 2004, doi: 10.1016/j.colsurfa.2004.02.014.
[19] R. A. Espinoza-González, D. E. Diaz-Droguett, J. I. Avila, C. A. Gonzalez-Fuentes, and V. M. Fuenzalida, "Hydrothermal growth of zirconia nano bars on zirconium oxide," *Mater. Lett.*, vol. 65, no. 14, 2011, doi: 10.1016/j.matlet.2011.04.056.
[20] A. Dittmar, D. L. Hoang, and A. Martin, "TPR and XPS characterization of chromia-lanthana-zirconia catalyst prepared by impregnation and microwave plasma enhanced chemical vapour deposition methods," *Thermochim. Acta*, vol. 470, no. 1–2, 2008, doi: 10.1016/j.tca.2008.01.019.
[21] S. L. Pal, U. Jana, P. K. Manna, G. P. Mohanta, and R. Manavalan, "Nanoparticle: An overview of preparation and characterization," *J. Appl. Pharm. Sci.*, vol. 1, no. 6, 2011.
[22] W. Xiao *et al.*, "Effect of urea as pore-forming agent on properties of poly (vinylidene fluoride-co-hexafluoropropylene)-based gel polymer electrolyte," *J. Power Sources*, vol. 252, pp. 14–20, 2014.
[23] S. F. Hasany, I. Ahmed, R. J, and A. Rehman, "Systematic Review of the Preparation Techniques of Iron Oxide Magnetic Nanoparticles," *Nanosci. Nanotechnol.*, vol. 2, no. 6, 2013, doi: 10.5923/j.nn.20120206.01.
[24] C. M. Hussain, *Handbook of Nanomaterials in Analytical Chemistry: Modern Trends in Analysis*. Elsevier, 2019.
[25] H. Qiu, L. Lv, B. C. Pan, Q. J. Zhang, W. M. Zhang, and Q. X. Zhang, "Critical review in adsorption kinetic models," *Journal of Zhejiang University: Science A*, vol. 10, no. 5. 2009. doi: 10.1631/jzus.A0820524.
[26] X. Dou, D. Mohan, C. U. Pittman Jr, and S. Yang, "Remediating fluoride from water using hydrous zirconium oxide," *Chem. Eng. J.*, vol. 198, pp. 236–245, 2012.
[27] F. Bondioli, A. Bonamartini Corradi, A. M. Ferrari, and C. Leonelli, "Synthesis of zirconia nanoparticles in a continuous-flow microwave reactor," *J. Am. Ceram. Soc.*, vol. 91, no. 11, 2008, doi: 10.1111/j.1551-2916.2008.02666.x.
[28] E. Rubio, V. Rodriguez-Lugo, R. Rodriguez, and V. M. Castano, "Nano zirconia and sulfated zirconia from ammonia zirconium carbonate," *Rev. Adv. Mater. Sci.*, vol. 22, no. 1–2, 2009.
[29] X. Zhao, Y. Zhang, S. Pan, X. Zhang, W. Zhang, and B. Pan, "Utilization of gel-type polystyrene

host for immobilization of nano-sized hydrated zirconium oxides: A new strategy for enhanced phosphate removal," *Chemosphere*, vol. 263, p. 127938, 2021.
[30]U. Lohbauer *et al.*, "Zirconia nanoparticles prepared by laser vaporization as fillers for dental adhesives," *Acta Biomater.*, vol. 6, no. 12, pp. 4539–4546, 2010.
[31]C. Y. Tai, M.-H. Lee, and Y.-C. Wu, "Control of zirconia particle size by using two-emulsion precipitation technique," *Chem. Eng. Sci.*, vol. 56, no. 7, pp. 2389–2398, 2001.
[32]J.-P. Simonin, "On the comparison of pseudo-first order and pseudo-second order rate laws in the modeling of adsorption kinetics," *Chem. Eng. J.*, vol. 300, pp. 254–263, 2016.
[33]Y.-S. Ho and G. McKay, "Pseudo-second order model for sorption processes," *Process Biochem.*, vol. 34, no. 5, pp. 451–465, 1999.
[34]E. D. Revellame, D. L. Fortela, W. Sharp, R. Hernandez, and M. E. Zappi, "Adsorption kinetic modeling using pseudo-first order and pseudo-second order rate laws: A review," *Clean. Eng. Technol.*, vol. 1, p. 100032, 2020.
[35]S. Malamis and E. Katsou, "A review on zinc and nickel adsorption on natural and modified zeolite, bentonite and vermiculite: Examination of process parameters, kinetics, and isotherms," *Journal of Hazardous Materials*, vol. 252–253. 2013. doi: 10.1016/j.jhazmat.2013.03.024.
[36]A. Sari, M. Tuzen, D. Citak, and M. Soylak, "Adsorption characteristics of Cu(II) and Pb(II) onto expanded perlite from aqueous solution," *J. Hazard. Mater.*, vol. 148, no. 1–2, 2007, doi: 10.1016/j.jhazmat.2007.02.052.
[37]K. Saltali, A. Sari, and M. Aydin, "Removal of ammonium ion from aqueous solution by natural Turkish (Yi{dotless}ldi{dotless}zeli) zeolite for environmental quality," *J. Hazard. Mater.*, vol. 141, no. 1, 2007, doi: 10.1016/j.jhazmat.2006.06.124.
[38]D. Karadag, Y. Koc, M. Turan, and B. Armagan, "Removal of ammonium ion from aqueous solution using natural Turkish clinoptilolite," *J. Hazard. Mater.*, vol. 136, no. 3, 2006, doi: 10.1016/j.jhazmat.2005.12.042.
[39]H. Zheng, Y. Wang, Y. Zheng, H. Zhang, S. Liang, and M. Long, "Equilibrium, kinetic and thermodynamic studies on the sorption of 4-hydroxyphenol on Cr-bentonite," *Chem. Eng. J.*, vol. 143, no. 1–3, pp. 117–123, 2008.
[40]K. M. Doke and E. M. Khan, "Adsorption thermodynamics to clean up wastewater; critical review," *Rev. Environ. Sci. Bio/Technology*, vol. 12, no. 1, pp. 25–44, 2013.